Title

Evaluating the effect of phosphorylation on the structure and dynamics of Hsp27 dimers by means of ion mobility mass spectrometry

Authors and Affiliations

Blagojce Jovcevski[1], Megan A. Kelly[1], J. Andrew Aquilina[1], Justin L. P. Benesch[2] and Heath Ecroyd[1]

[1]Illawarra Health and Medical Research Institute and School of Biological Sciences, University of Wollongong, Wollongong, New South Wales 2522, Australia

[2]Department of Chemistry, Physical and Theoretical Chemistry Laboratory, South Parks Road, Oxford OX1 3QZ, United Kingdom

Corresponding Author

Email: heathe@uow.edu.au (H.E.); Ph: 61-2-4221-3443

Keywords

Small heat-shock proteins; molecular chaperones; proteostasis; phosphorylation; native mass spectrometry; Hsp27, HSPB1; protein aggregation; ion mobility – mass spectrometry

Abstract

The quaternary structure and dynamics of the human small heat-shock protein Hsp27 is linked to its molecular chaperone function and influenced by post-translational modifications, including phosphorylation. Phosphorylation of Hsp27 promotes oligomer dissociation and can enhance chaperone activity. This study explored the impact of phosphorylation on the quaternary structure and dynamics of Hsp27. Using mutations that mimic phosphorylation and ion mobility mass spectrometry we show that successive substitutions result in an increase in the conformational heterogeneity of Hsp27 dimers. In contrast, we did not detect any changes in the structure of an Hsp27 12mer, representative of larger Hsp27 oligomers. Our data suggests that oligomer dissociation and increased flexibility of the dimer contribute to the enhanced chaperone activity of phosphorylated Hsp27. Thus, post-translational modifications, such as phosphorylation, play a crucial role in modulating both the tertiary and quaternary structure of Hsp27, which is pivotal to its function as a key component of the proteostasis network in cells. Our data demonstrates the utility of ion mobility mass spectrometry for probing the structure and dynamics of heterogeneous proteins.

TOC Graphic

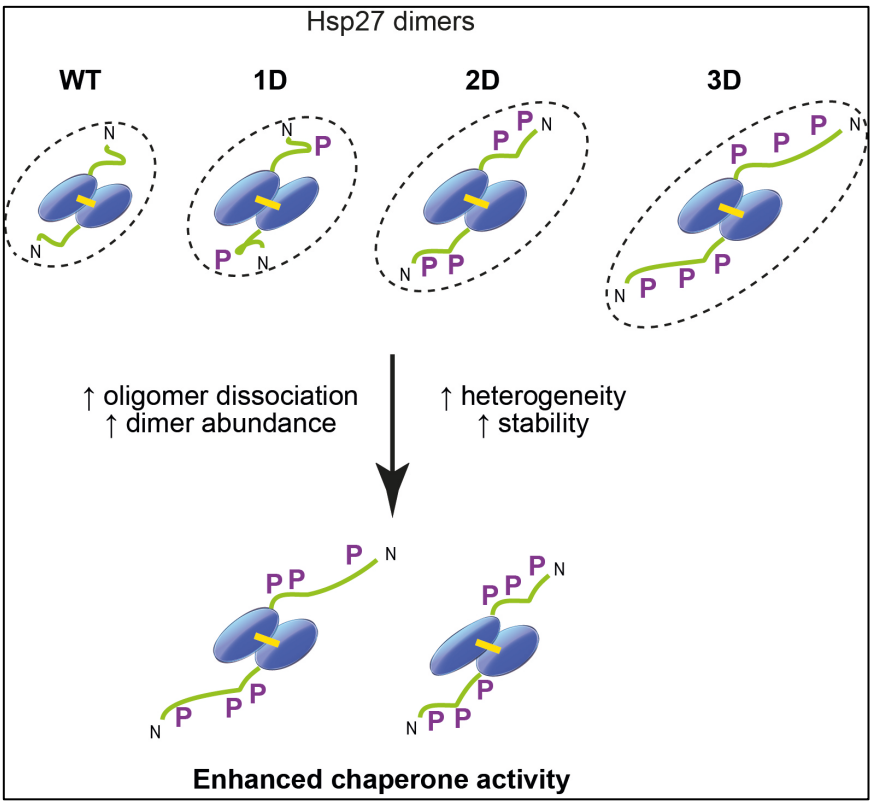

Introduction

Hsp27 (HSPB1) is a mammalian small heat-shock protein (sHsp) that is constitutively expressed in muscle, neuronal and cancer cells[1,2]. Hsp27 forms large polydisperse oligomers[3,4] and the amount of Hsp27 in cells increases dramatically during periods of cell stress[5]. Through its roles in preventing protein aggregation[3,6-9], stabilising the cytoskeleton[10,11] and inhibiting apoptosis[12,13], Hsp27 plays a key role in maintaining protein homeostasis (proteostasis) in cells. Moreover, mutations in Hsp27 are associated with diseases such as Charcot-Marie Tooth disease and distal hereditary motor neuropathies[14-16].

It is generally accepted that the quaternary structure and dynamics of sHsps are linked to their molecular chaperone function[17-20]. However, little focus has been placed on the quaternary structure and dynamics of Hsp27, despite its role in a range of cellular functions. In addition, Hsp27 undergoes stress-induced phosphorylation at three serine residues (S15, S78 and S82) in its N-terminal region, which regulates its assembly and chaperone function[21,22]. Moreover, the oligomeric state of Hsp27 is modulated by both concentration and post-translational modifications[23,24]. Our previous work investigated the effect of phosphorylation on the structure and function of Hsp27 using mutations that mimic phosphorylation (MMP). We demonstrated that the dissociation of oligomers and

chaperone activity was enhanced with an increasing number of MMPs[23]. As a result, we proposed that the dimer is the chaperone-active unit of Hsp27, however, it was unclear whether the dissociation of oligomers into dimers (i.e. changes in quaternary structure) or phosphorylation-induced changes in the conformation and/or dynamics of the dimer itself (i.e. changes in tertiary structure), or both, are responsible for the enhanced chaperone activity of phosphorylated Hsp27. Moreover, there has been little work conducted to date exploring the structural dynamics of Hsp27 at the tertiary and quaternary level.

Native mass spectrometry (MS) offers great potential for the study of multimeric protein assemblies, and has been successfully used to study the quaternary organisation of various sHsps, including Hsp27[6,23,25-28]. Native MS allows the interrogation of the structure and dynamics of individual species present in a complex mixture, which cannot be achieved with standard biophysical approaches that average over all species in solution. Here we capitalised on the capabilities of IM-MS to explore the impact phosphorylation has on the tertiary and quaternary structure and dynamics of Hsp27. To investigate the effect of phosphorylation, isoforms of Hsp27 with MMP ($Hsp27_M$) were examined by IM-MS to ascertain the conformational state of two oligomeric forms, dimers and 12mers, the latter as a representative of large oligomers formed by Hsp27. In addition, the unfolding dynamics of Hsp27 dimers was examined via collision-induced unfolding (CIU) in order to observe any differences in the unfolding of dimers with MMP. Our data are consistent with phosphorylation regulating the conformational heterogeneity and stability of Hsp27 dimers.

Experimental Section

Protein Expression and Purification. The gene encoding human Hsp27 (*HSPB1;* UniProt accession number P04792) was expressed in *E. coli* BL21(DE3) using a plasmid kindly gifted by Drs. W. C. Boelens and W. W. de Jong (University of Nijmegen, The Netherlands), in which *HSPB1* was cloned into the *Bam*HI and *Nde*I restriction sites of pET3a (Novagen). The Hsp27 phosphomimic-encoding plasmids (S15D, S15/82D and S15/78/82D) were generated by site-directed mutagenesis of the wild-type-containing plasmid by GenScript (Piscataway, NJ, USA). Expression and purification of each recombinant protein was performed as described previously[6,29].

Analytical-SEC. The oligomeric size of Hsp27-WT and $Hsp27_M$ was determined by analytical-SEC. Samples (50 μM) were loaded onto a Superdex 200 10/300 GL analytical size-exclusion column (GE Healthcare), which had been equilibrated in 200 mM ammonium acetate (NH_4OAc) (pH 6.8), at a flow rate of 0.4 mL/min at room temperature. The size-exclusion columns were calibrated using standards (Bio-Rad): bovine thyroglobulin (670 kDa), bovine γ-globulin (158 kDa), chicken ovalbumin (44 kDa) and horse myoglobin (17 kDa).

Intrinsic tryptophan fluorescence. Intrinsic tryptophan fluorescence was used to examine changes in the tertiary and quaternary structure of Hsp27 (Hsp27 contains the following tryptophan residues; W16, W22, W42, W45, W51 and W95). Tryptophan fluorescence spectra were attained using a Cary Eclipse fluorescence spectrophotometer (Varian, USA). Proteins were prepared to a final concentration of 50 μM in 200 mM NH_4OAc (pH 6.8). Proteins were incubated at room temperature for 15 min prior to tryptophan fluorescence analysis. The excitation wavelength was set at 295 nm and 350 nm and emission wavelength was recorded from 300-400 nm. Slit widths for excitation and emission spectra were both set at 5 nm.

Bulk-FRET monitoring of subunit exchange. Bulk-FRET was used to determine whether Hsp27-WT and Hsp27-3D were capable of subunit exchange. Hsp27-WT was labelled with CF-488A (Sigma-Aldrich) and CF-647 succinimidyl ester dyes (Biotium) and Hsp27-3D was labelled with CF-488A (Sigma-Aldrich) succinimidyl ester dye. Individual stocks of labelled proteins were made up to 25 μM in 50 mM phosphate buffer (pH 7.4). Samples were equilibrated by incubation at 37°C for 1 h and placed on ice for 20 min to halt subunit

exchange[30]. Subunit exchange was monitored using a POLARstar plate reader (BMG Lab Technologies) based on the change in FRET over time. Equimolar ratios of the putative subunit-exchange pairs (i.e. Hsp27-WT-488 + Hsp27-3D-647; Hsp27-WT-488 + Hsp27-WT-647) were plated (in duplicate) into a black 384-microwell plate and FRET monitored for 90 min at 37°C by measuring the levels of fluorescence with a 490/650 nm excitation/emission filter set. The ratio of fluorescence intensity at any point in time, $F(t)$, to fluorescence intensity at time zero, $F(0)$, was calculated, i.e. $F(t)/F(0)$. An increase in this fluorescence ratio was indicative of subunit exchange. Subsequent reaction curves were fitted with a one-phase association (exponential) curve to determine the subunit-exchange rate constant (k). Subunit exchange was also confirmed by analytical-SEC whereby samples were taken directly from the 384-well microplates and loaded onto a Superdex 200 10/300 GL analytical-SEC pre-equilibrated with 50 mM phosphate buffer (pH 7.4) with multi-wavelength detection set at 280, 495 and 650 nm and eluted at 0.3 mL/min.

Ion mobility mass spectrometry. IM-MS was performed on a Synapt G1 HDMS (Waters) using a nanoelectrospray ionisation source following a previously described protocol[31]. Prior to all MS analyses, Hsp27-WT and $Hsp27_M$ were buffer-exchanged using a Superdex 200 10/300 GL analytical size-exclusion column (GE Healthcare), which had been equilibrated in 200 mM NH_4OAc (pH 6.8), at a flow rate of 0.4 mL/min at room temperature. Protein concentration was adjusted to 50 µM for IM-MS experiments and 2 µL of protein was loaded onto gold-coated borosilicate glass capillaries prepared in-house. To investigate the quaternary architecture of Hsp27 assemblies, gentle source conditions were required to minimise gas-phase compaction and unfolding prior to detection. Key instrument parameters were as follows: capillary voltage (kV): 1.60-1.65; sampling cone (V): 40; extraction cone (V): 2.0; trap/transfer collision energy (V): 15/10; trap gas (L/hr): 6.0; backing gas (mbar): ~6.5. The parameters for the IM were as follows: IM cell wave height (V): 8-10; IM cell wave velocity (m/s): 300; transfer t-wave height (V): 8; transfer t-wave velocity (m/s): 200.

The IM data for the large oligomer (12mer) was acquired as described previously[32,33]. Key instrument parameters were as follows: capillary voltage (kV): 1.60-1.65; sampling cone (V): 40; extraction cone (V): 2.0; trap/transfer collision energy (V): 15/10; trap gas (L/hr): 6.0; backing gas (mbar): ~6.5. IM parameters were as follows: IM cell wave height (V): 10-14.5;

IM cell wave velocity (m/s): 300; transfer wave height (V): 8; transfer wave velocity (m/s): 200. Arrival time distribution (ATD) data was acquired and calculated using Driftscope 2.1 (Waters) as described previously[32].

Collision-induced unfolding (CIU). To investigate the CIU dynamics of Hsp27 dimers, given that all the single phosphomimic isoforms were structurally and functionally similar (as were all the double phosphomimic isoforms)[23], the S15D, S15/82D and S15/78/82D mutants were selected as representatives of the 1D, 2D and 3D isoforms respectively (referred to as Hsp27-1D, Hsp27-2D and Hsp27-3D). In these experiments the 13+ dimer was selected to minimize overlap from other species, and IM spectra was acquired under the conditions stated above. A power-calculation used to determine an appropriate charge state for CIU analysis (which is dependent on the molecular mass)[34] indicated that the 13+ charge state is suitable for investigating the CIU of Hsp27 dimers (power-calculation gave the optimal charge state as 12+). The trap and transfer collision energy was increased in 5 V increments from 15 – 60 V. IM heat maps and CIU difference plots were generated using CIUsuite with default settings[35]. To determine the relative proportion of unfolded dimer with increasing activation energy, IM chromatograms at each activation energy increment were measured and normalised to the highest intensity. The relative abundance of unfolded dimer was determined by the intensity of any unfolded species present (i.e. any observed intensity that is not attributed to the folded dimer).

Results

Using bulk measurement techniques to identify changes in Hsp27 tertiary and quaternary structure with serine substitutions that mimic phosphorylation. The increased abundance of Hsp27 dimers with MMP strongly correlates with enhanced chaperone activity[23]. To determine whether other changes occur to the tertiary and quaternary structure of Hsp27 upon introduction of MMP, biophysical studies were conducted on these isoforms. Intrinsic tryptophan fluorescence studies revealed that all $Hsp27_M$ isoforms (i.e. those containing one, two or three MMP) had an enhanced tryptophan fluorescence intensity compared to Hsp27 wild-type (WT), consistent with increased solvent exposure of one or more tryptophan residues (Hsp27 has six tryptophan residues; W16, W22, W42, W45, W51 and W95) (Figure 1A-B). However, this was not accompanied by a shift in the maximum emission wavelength (Figure 1A-B). Analytical-size exclusion chromatography (SEC) of $Hsp27_M$ in ammonium acetate (NH_4OAc) (i.e. the buffer used for all the MS experiments), in general mirrors the results obtained when phosphate buffer was used[23]. An increase in the number of MMP reduces the size of Hsp27 oligomers (Figure 1C-D); which was observed previously when the samples were analysed in phosphate buffer[23]. Single $Hsp27_M$ isoforms eluted in two distinct peaks, one with an elution volume similar to that of Hsp27-WT (~590 kDa) and a relatively small proportion that eluted in a peak corresponding to a molecular mass of ~45 kDa (Figure 1C). The proportion of the ~45 kDa species, relative to the large 590 kDa species, increased significantly for the double $Hsp27_M$ isoforms (Figure 1D). Hsp27-S78/82D exhibited the largest proportion of smaller oligomers (45 – 158 kDa) across all the double $Hsp27_M$ isoforms studied. The triple phosphomimic (Hsp27-S15/78/82D; Hsp27-3D) eluted as a single species ~45 kDa, corresponding to the mass of a dimer (Figure 1C-D). A potential reason for the variation in elution profiles compared to our previous work[23] could be due to the differences in the buffer systems (phosphate buffer with a pH of 7.4 was used previously whereas this work was conducted in the MS-compatible buffer ammonium acetate and a pH of 6.8 to replicate that used in the MS experiments). Other studies have shown that small differences in pH can cause significant differences in quaternary dynamics of sHsps[36], while the sensitivity of sHsps to buffer composition has also been noted[37,38] . However, both sets of data are clearly consistent with an increase in the dissociation of Hsp27 oligomers into dimers with increasing MMP.

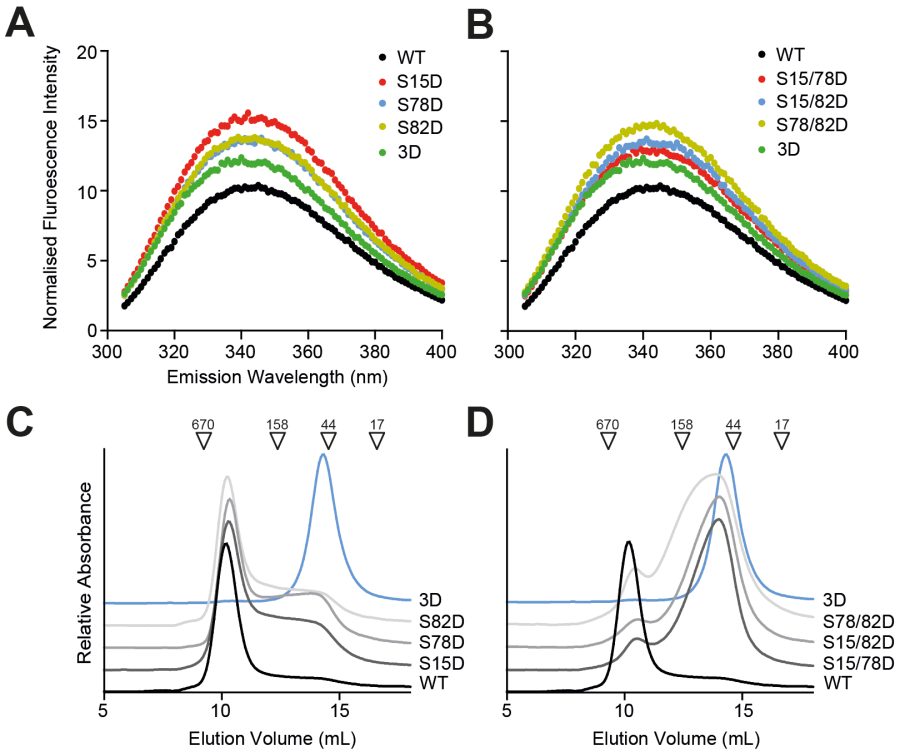

Figure 1: Intrinsic tryptophan fluorescence and analytical size-exclusion chromatography of Hsp27$_M$. *A-B*: Intrinsic tryptophan fluorescence of single Hsp27$_M$ (***A***) and double Hsp27$_M$ (***B***) isoforms (50 µM) in 200 mM ammonium acetate (NH_4OAc) buffer (pH 6.8) showing an increase in tryptophan exposure relative to Hsp27-WT. ***C-D*:** Analytical-SEC of single Hsp27$_M$ (***C***) and double Hsp27$_M$ (***D***) (50 µM) in 200 mM NH_4OAc (pH 6.8) where successive serine substitutions enhance oligomer dissociation. Both Hsp27-WT and Hsp27-3D are also included for relative comparison in all panels. Elution volume of molecular weight standards are indicated above the chromatograms (in kDa).

Hsp27-3D and Hsp27-WT undergo subunit exchange. In order to elucidate whether phosphorylated dimers of Hsp27 (Hsp27-S15/78/82D: Hsp27-3D) could be incorporated into oligomers of non-phosphorylated Hsp27 (Hsp27-WT), we performed a bulk-FRET assay to monitor subunit exchange between these two isoforms. It was observed that Hsp27-3D was capable of subunit exchange with Hsp27-WT, and the rate of exchange (0.2740 ± 0.02 min^{-1}) was faster than that of WT homo-oligomers (0.2289 ± 0.01 min^{-1}) (Figure 2A). To confirm that Hsp27-3D was incorporated into large oligomers formed by Hsp27-WT, samples from the bulk-FRET experiments were collected and analysed by analytical-SEC with multi-wavelength detection. Analytical-SEC showed that the mixed sample of Hsp27-WT and -3D

resulted in a peak eluting from the column at an elution volume typical of large Hsp27 oligomers (~8 mL), and that this peak contained both Hsp27 isoforms (Figure 2B-C).

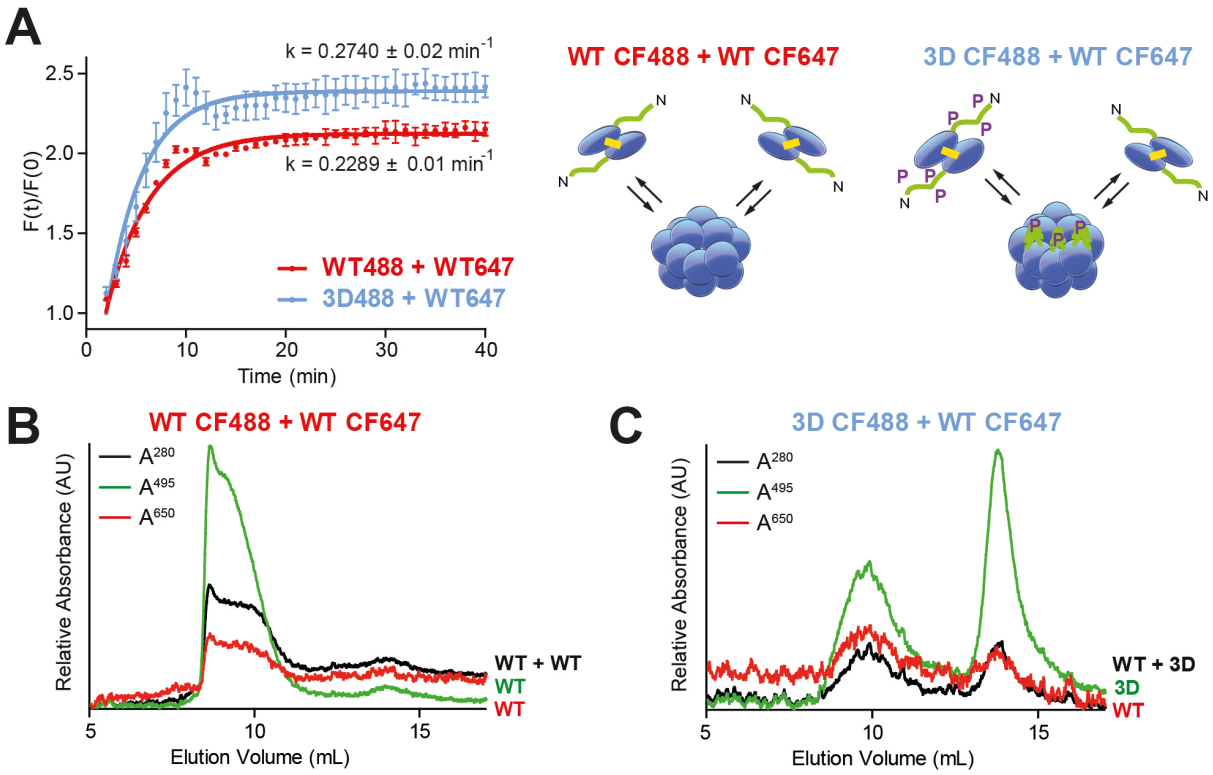

Figure 2: Hsp27-WT and Hsp27-3D are capable of undergoing subunit exchange. *A*: Bulk-FRET assays indicating that subunit-exchange of Hsp27-WT with Hsp27-3D occurs at a rate faster than WT exchange (*left panel*). Subunit exchange was performed at 37 °C at a 1:1 molar ratio (25 µM total protein concentration) in 50 mM phosphate buffer (pH 7.4). The emission fluorescence from Alexa labels was used as a measure of subunit exchange. A general schematic of subunit exchange between homo- and hetero-oligomeric forms are as indicated (*right panel*). Bulk-FRET data is the mean ratio in fluorescence intensity ± standard error of the mean of three independent experiments. ***B*:** Analytical-SEC of Hsp27-WT (CF488) with Hsp27-WT (CF647) after bulk-FRET subunit exchange ***C*:** Analytical-SEC of Hsp27-3D (CF488) with Hsp27-WT (CF647) after bulk-FRET subunit exchange. Both **B** and **C** were at a 1:1 molar ratio (25 µM total protein concentration) in 50 mM phosphate buffer (pH 7.4). Absorbance of Hsp27-WT and Hsp27-3D was measured at multiple wavelengths (280 nm: *black*; 495 nm: *green*; 650 nm: *red*).

Increased serine substitutions alter the conformation and unfolding dynamics of Hsp27 dimers. Characterising the secondary, tertiary and quaternary structure of partially disordered proteins using bulk-averaged methods only provides relatively low-resolution structural information which is unable to discriminate between individual oligomeric states. As a result, alternate approaches are required to probe the structure of these assemblies with greater resolution. IM-MS is an extremely useful tool to analyse the size, shape and conformation of folded proteins in various states (e.g. unfolded/folded)[39]. By isolating a particular species of interest, in this case the dimer^{13+} (~3,510 *m/z*) and the 12mer^{31+} (~8,800 *m/z*), both corresponding to unique mass to charge ratios (i.e. this charge-state peak does not overlap charges states of other populated stoichiometries), differences in these oligomeric forms (in terms of shape and conformation), with increasing numbers of MMP, can be probed (Figure 3A). In addition, as IM-MS is sensitive to the folding states of proteins, it also enables the unfolding of proteins in the gas-phase to be observed. During IM-MS, an increase in activation energy leads to CIU, which can be observed as an increase in arrival time[40]. Thus, the unfolding process can be visualised to determine distinct conformations that a protein may transition through (i.e. native, compaction, intermediately folded and unfolded), as well as determine the relative stability of a species as a function of activation energy.

We sought to compare the arrival time distribution (ATD) of the Hsp27 dimer^{13+} with successive MMPs at a set height (WH) under low activation energy and gentle source conditions (i.e. native-like state; Figure 3B-C). Hsp27-WT was not able to be included in this analysis as the proportion of free dimer in solution at the concentrations required for this experiment (50 µM; monomeric concentration) was too low to be detected under the instrument settings used in these experiments. In addition, all the single Hsp27$_M$ isoforms have been shown to be structurally and functionally similar (as were all the double Hsp27$_M$ isoforms)[23], and thus the S15D, S15/82D and S15/78/82D mutants were selected as representatives of the 1D, 2D and 3D isoforms respectively (referred to herein as Hsp27-1D, Hsp27-2D and Hsp27-3D). The data from these Hsp27$_M$ isoforms demonstrates that the tertiary structure of Hsp27 dimers changes with successive MMP. The dimer ATD was observed to broaden with an increasing number of MMP (Figure 3B; inset) (Table S1). These data are consistent with increased heterogeneity in the ensemble of states able to be

accessed by Hsp27 dimers with MMP. In contrast, there was no distinct shift in either the centroid of breadth of the ATD observed for the $12mer^{31+}$ between the $Hsp27_M$ and Hsp27-WT isoforms (Figure 3C; inset). This is consistent with the N-terminal region of the Hsp27 being on inside of the 12mers, such that the tertiary structure changes we observed in the dimer do not impact the overall collision cross-section of the oligomer. Hsp27-3D was not able to be used in this latter experiment as we have previously shown that it is predominantly dimeric[23]. Overall, the data demonstrates that MMP alter the tertiary structure of Hsp27 dimers, making them more heterogeneous (and by inference flexible) with successive MMP.

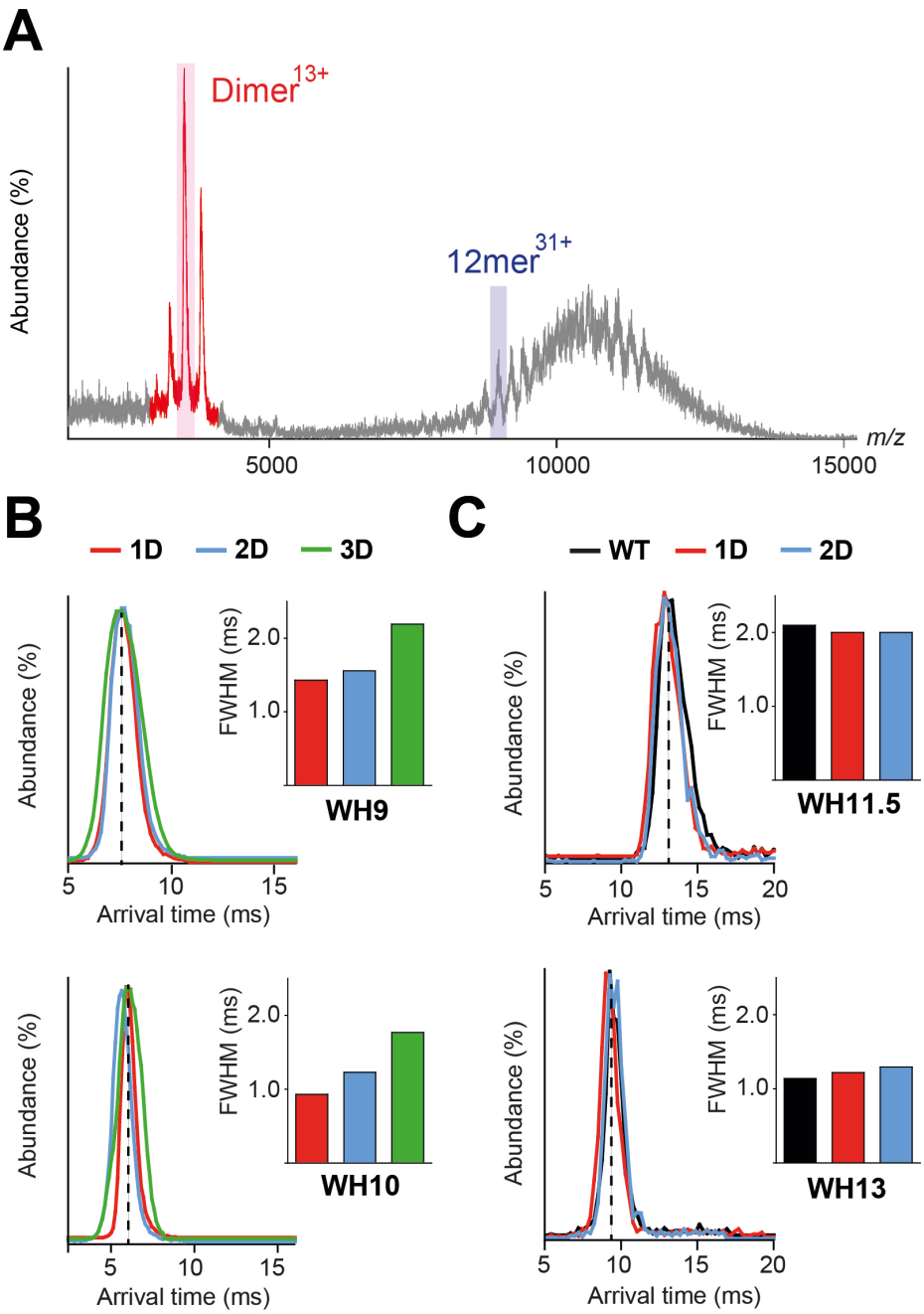

Figure 3: Arrival time distribution analysis and collision-induced unfolding trajectories of Hsp27 using ion mobility – mass spectrometry. ***A*:** Native MS of Hsp27-S15D under low activation energy (15 V), demonstrating the approach used to observe the conformation and unfolding dynamics of Hsp27 dimers. The 13+ charge state of dimers (3,510 *m/z*; *red box*) and the 31+ charge state of the 12mer (8,800 *m/z*, *blue box*) were selected for analysis. ***B*:** ATD analysis of $Hsp27_M$ dimers^{13+} at low activation energy (15 V) and a range of wave heights (WH in V) showing that the structure of the dimer is more heterogenous (broadness of the peak; inset) with an increasing number of MMP. ***C*:** ATD analysis of Hsp27-WT and

$Hsp27_M$ $12mers^{31+}$ at low activation energy (15 V) and two WH which shows that the arrival time and broadness of the peak (and hence conformation; inset) of the 12mer does not vary significantly with increasing numbers of MMP.

To probe potential differences in the structure of $Hsp27_M$ dimers further, IM-MS was used to monitor the unfolding of these dimers at different WHs by means of CIU. By increasing the acceleration into the collision cell of the mass spectrometer, whilst maintaining low activation energy in the source, the unfolding of Hsp27 dimers was monitored (Figure 4). Across all isoforms, it appears that both monomeric units within the (disulfide-bonded) dimer unfold simultaneously, i.e. there is no evidence of one monomer unfolding prior to the other as only a single conformation/species is observed after 40 V (two unfolding events would be observed with increasing activation energy if one monomer unfolded prior to the other) (Figure 4B, S1A, S1D). In addition, a slight compaction of the dimer (evidenced by a decrease in the ATD) was evident for the Hsp27-2D and Hsp27-3D isoforms at 30 V and WH8 (Figure 4B, 4D), WH9 (Figure S1B) and WH10 (Figure S1D-E), prior to unfolding. However, the amount of activation energy required to unfold the dimer increases when the third MMP is present, such that Hsp27-3D is the most resistant to unfolding of all the Hsp27 isoforms (45 V at WH8 and WH9, compared to 40 V for Hsp27-1D and 2D at these wave heights) (Figure 4B, S1A, S1C, S1F).

In order to determine the differences in the CIU of Hsp27 dimers, pair-wise comparisons of $Hsp27_M$ isoforms (i.e. Hsp27-1D versus -2D and Hsp27-1D versus -3D etc.) were generated. These enabled quantitative differences in the ATD of the unfolding dimer with increasing activation energy to be measured (Figure 4D, S1B, S1D). Interestingly, the folded and unfolded states of Hsp27-3D differ when compared to Hsp27-1D and -2D across multiple wave heights; more activation energy is required for the unfolding of the Hsp27-3D dimer compared to the Hsp27-1D or -2D dimers (Figure 4D, S1B, S1D). The unfolding trajectories of Hsp27-1D and Hsp27-2D, compared to Hsp27-3D, at WH8 resulted in a RMSDs of 11.34 % and 9.69 %, respectively (the RMSD of independent trajectories of the same protein was 5.44 %; Figure S2) (Figure 4D). This indicates that the unfolding pathway of Hsp27-3D differs substantially to that of Hsp27-1D and Hsp27-2D. Overall, these data suggest that the negative charges introduced by MMPs are involved in electrostatic interactions within

Hsp27 dimers, resulting in the dimer being more resistant to unfolding. In addition, the data also demonstrates that IM-MS is a sensitive technique to detect such electrostatic interactions within heterogeneous proteins.

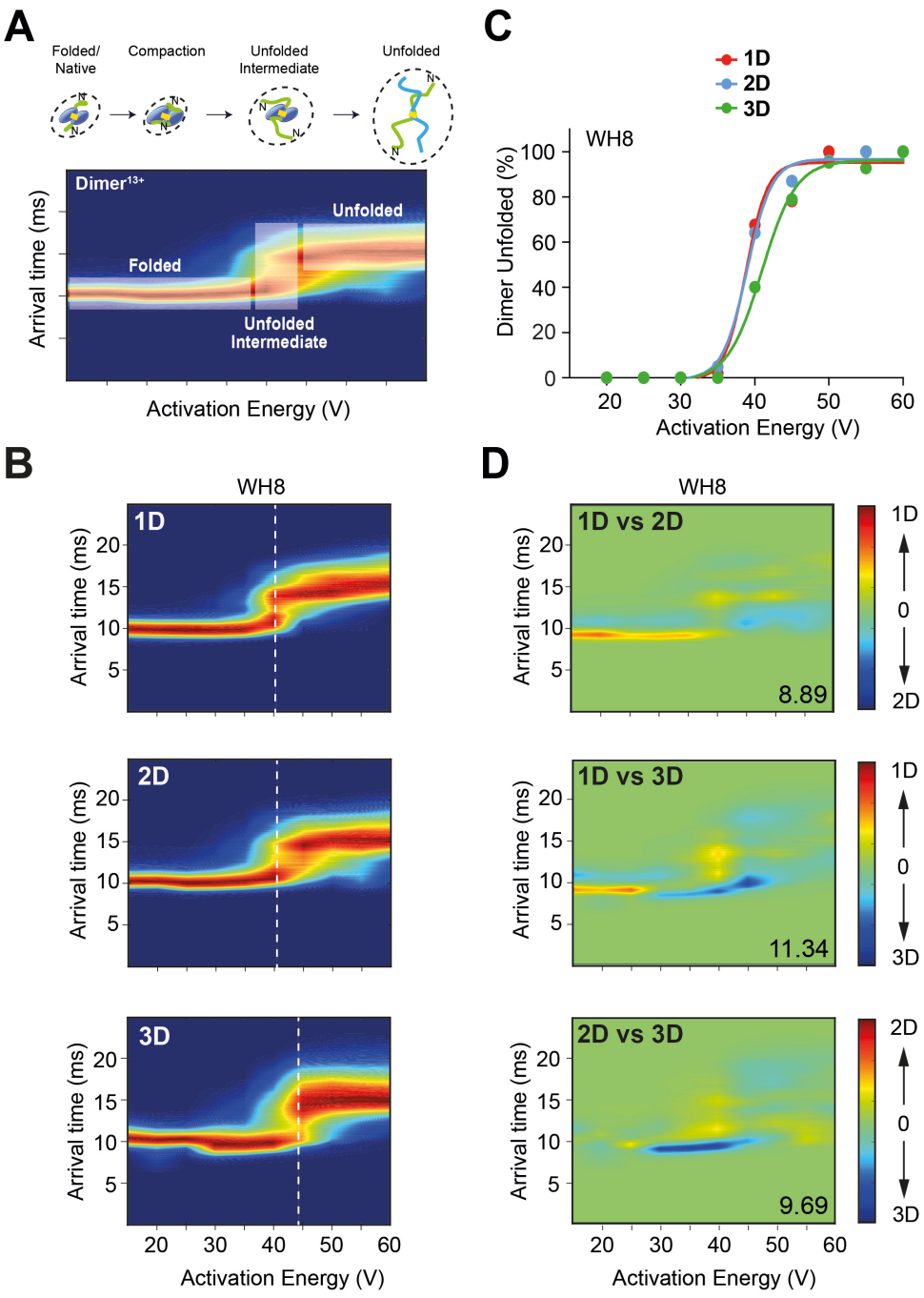

Figure 4: Observing the collision-induced unfolding of Hsp27$_M$ dimers by IM-MS. ***A:*** The various conformations that Hsp27 dimers adopt in the gas-phase under low activation energy. The increase in activation (collision) energy results a slight compaction of dimers, which then unfold with further increases in activation energy. The unfolding intermediates

can be observed prior to complete unfolding of the dimer (a generic collision-induced unfolding, CIU, pathway is illustrated above the heat map). ***B:*** The CIU of the $Hsp27_M$ $dimer^{13+}$ (monitored via changes in the arrival time of species in the IM chamber) was examined with increasing activation energy (V). The heat maps indicate that no distinct intermediate species (i.e. no partially structured intermediate) between folded and unfolded states are present as the dimer unfolds in the gas-phase as a function of activation energy at the same wave height (WH in V) (WH8). Across all wave heights, only a single unfolding transition is observed (*white dashed line*), indicating that both monomers (which are disulfide-linked via Cys137) unfold simultaneously in the gas-phase. ***C:*** The abundance of unfolded dimer (y-axis) was determined by tracking the loss of folded dimer with increased activation energy as a set wave height (WH8). The Hsp27-3D dimer appears to be more stable (i.e. requires increased activation energy to reach 50% unfolded) compared to the –1D and -2D isoforms. ***D:*** Heat maps generated by using the CIUsuite_compare function which highlight the differences in the unfolding of the $dimer^{13+}$ in the gas-phase between two isoforms at the same wave height (WH8). Difference plots are shown whereby features that identify most strongly with one fingerprint are shown on a red intensity scale and the other is shown in blue. RMSDs (%) (*bottom right corner*) indicate the difference in the unfolding of the dimer between each pair analysed. Hsp27-1D vs Hsp27-2D (*top*), Hsp27-1D vs Hsp27-3D (*middle*) and Hsp27-2D vs Hsp27-3D (*bottom*) are shown. The greatest difference in the unfolding dynamics was observed when Hsp27-1D or Hsp27-2D were compared with Hsp27-3D.

Discussion

The role of Hsp27 in intracellular proteostasis is inherently linked to its structural dynamics, whereby changes in structure at the tertiary and quaternary level modulate its chaperone activity. We have previously utilised MMP to investigate the site-specific role phosphorylation has on the structure and chaperone function of Hsp27, reporting that increased levels of phosphorylation induce oligomer dissociation into dimers which correlates to enhanced chaperone activity[23]. The work presented here aimed to define the conformation and dynamics of Hsp27 oligomers, in particular, chaperone-active dimers.

Many biophysical approaches, such as intrinsic tryptophan fluorescence and analytical-SEC used here, only provide low-resolution structural information on proteins that is limited when dealing with large heterogeneous assemblies such as the sHsps. Whilst we observed enhanced tryptophan exposure with MMP compared to WT (Figure 1A-B), our analytical-SEC data indicates that there is an increased abundance of smaller Hsp27 isoforms with MMP. As it was not possible to discern between individual oligomeric species with these ensemble-averaging approaches, these changes in tryptophan exposure cannot be attributed to a particular species. Thus, the increase in tryptophan fluorescence intensity with MMP may reflect either an increase in the proportion of dissociated species that arise due to these mutations (i.e. changes in quaternary structure) or changes in the environment of the tryptophan residues in the oligomers themselves (i.e. changes in tertiary structure). Interestingly, as there was no accompanying shift in the maximum emission wavelength upon MMP, fluorescence quenching may be responsible for the lower tryptophan fluorescence observed for Hsp27-WT. Of note, five of the six tryptophan residues in Hsp27 reside in the N-terminal domain, and one (W16) is immediately adjacent to S15, a site of phosphorylation in Hsp27 and modified by MMP in this work. Thus, the MMP may result in a decrease in localised quenching of tryptophan fluorescence leading to the increase in tryptophan fluorescence observed for all $Hsp27_M$ isoforms. However, other mechanisms that lead to a change in the quantum yield of tryptophan fluorescence are possible[41]. Due to the limitations present in using low resolution approaches to probe the structure and dynamics of Hsp27, we chose to use IM-MS which enables individual oligomeric species to be analysed within a complex mixture.

The overall findings of this work demonstrate that there are distinct differences in the structure of Hsp27 dimers as a result of MMP, whereby with an increasing number of MMP the Hsp27 dimer becomes more heterogeneous. Our data also suggest that the negative charges introduced by phosphorylation are involved in electrostatic interactions within the dimer, which would likely lead to an increase in stability of the dimer in solution. We conclude that these structural changes to the dimer upon phosphorylation likely contribute to enhanced chaperone activity[23] through increasing its capacity to interact with misfolded client proteins to attenuate aggregation.

As it was previously shown that MMP enhance oligomer dissociation of Hsp27, it was postulated that oligomeric disassembly is mediated by negative charge repulsion between dimers that result from phosphorylation[23]. We therefore tested whether Hsp27-3D was capable of being incorporated into large Hsp27-WT oligomers since the negative charge introduced to mimic phosphorylation in Hsp27-3D could prevent this from occurring. Bulk-FRET and SEC analysis demonstrated that Hsp27-3D is indeed capable of being incorporated into large Hsp27-WT oligomers[3]. This finding indicates that Hsp27 oligomers are able to accommodate negative charges introduced by phosphorylation, at least up to a point. We reason that there is a threshold at which the associative forces that hold the oligomer together are outweighed by the Coulombic repulsion caused by incorporation of increasing numbers of phosphate groups, eventually leading to dissociation of the Hsp27 oligomers, and that these factors contribute to the faster subunit exchange of Hsp27-3D. Whilst studies of αB-c using MMP have demonstrated that variant isoforms are also capable of subunit-exchange[37,42], phosphorylation of αB-c does not lead to the complete dissociation of oligomers (in contrast to Hsp27). Rather, the rate of subunit-exchange between αB-c oligomers increases substantially with MMP[37]. Thus, for both Hsp27 and αB-c, the population of dissociated species at any point in time is increased upon the introduction of MMP (and by inference phosphorylation), such that more chaperone-active units are available to interact with and prevent the aggregation of client proteins.

The ability to observe specific Hsp27 oligomeric forms by using native MS allowed us to specifically interrogate how the conformation of the full-length dimer varies due to MMP. By comparing the ATD of Hsp27 dimers between $Hsp27_M$ forms under identical IM-MS conditions, we conclude that MMP result in the broadening of the ATD peak width of the

dimer and an increase in the arrival time at some WHs. We did not detect any change in the shape or stability of the 12mer oligomer with MMP by IM-MS. Together these results suggest that, at the level of the dimeric building block, progressive serine phosphorylation of Hsp27 leads to increasing oligomeric dissociation. It also results in the dimer being able to access more conformations (i.e. being more flexible) with MMP.

Interestingly, the unfolding pathway (and by inference stability) of the Hsp27 dimer differed with an increase in the number of MMP, such that more energy was needed to unfold the Hsp27-3D dimer compared to the Hsp27-1D or -2D dimer. The likely explanation for this is that the negative charges introduced by phosphorylation (or in our case Asp residues to mimic phosphorylation) are involved in intra-dimer electrostatic interactions, making the dimer more resistant to unfolding in the gas phase, where these electrostatic interactions are strengthened[43,44]). Nevertheless, we reason these interactions must still originate in solution, and note that similar interactions have also been previously observed for another mammalian sHsp, Hsp20[45]. As such, we contend that our data demonstrates that IM-MS acts as a sensitive diagnostic means for detecting such interactions which are difficult to study in solution.

In summary, these data indicate that phosphorylation of Hsp27 results in changes to the tertiary structure of Hsp27 dimers, such that the dimer adopts more conformations (i.e. increasingly heterogeneous dimer) and that the N-terminal domain forms strong intra-dimer electrostatic interactions in solution. We postulate that these new intra-dimer interactions act to weaken the inter-dimer interactions, thereby precipitating disassembly of the oligomers. As a result, these changes lead to an enhanced ability of phosphorylated Hsp27 dimers to recognise and interact with misfolded and aggregating proteins. In summary, phosphorylation of Hsp27 result in structural changes at the tertiary and quaternary level, and these facilitate changes in Hsp27 chaperone activity in cells. In addition, the data also demonstrates the ability of IM-MS to probe the structure and dynamics of heterogeneous proteins, one stoichiometry at a time.

Author Contributions

B.J., J.A.A. and H.E. designed the research; B.J. and H.E. performed the experiments; B.J., J.L.P.B., and H.E. analysed experimental data; B.J., J.L.P.B., and H.E. wrote the manuscript.

Acknowledgments

B.J. is supported by an Australian Rotary Health/The Henning Family matching PhD scholarship. J.L.P.B. thanks the BBSRC for support of this project. H.E. was supported by an Australian Research Council Future Fellowship (FT110100586). This research used equipment funded by ARC LIEF Grant (LE0882289) located at the UOW Mass Spectrometry User Resource and Research Facility (MSURRF). We would like to thank the Illawarra Health and Medical Research Institute and MSURRF for technical support. We also wish to thank the reviewers for their insightful comments and suggestions, which have improved the manuscript.

References

(1) Jonak, C.; Mildner, M.; Klosner, G.; Paulitschke, V.; Kunstfeld, R.; Pehamberger, H.; Tschachler, E.; Trautinger, F. *J Dermatol Sci* **2011**, *61*, 32-37.

(2) Garrido, C.; Ottavi, P.; Fromentin, A.; Hammann, A.; Arrigo, A. P.; Chauffert, B.; Mehlen, P. *Cancer research* **1997**, *57*, 2661-2667.

(3) Rogalla, T.; Ehrnsperger, M.; Preville, X.; Kotlyarov, A.; Lutsch, G.; Ducasse, C.; Paul, C.; Wieske, M.; Arrigo, A. P.; Buchner, J.; Gaestel, M. *The Journal of biological chemistry* **1999**, *274*, 18947-18956.

(4) Garrido, C. *Cell Death Differ* **2002**, *9*, 483-485.

(5) Jakob, U.; Gaestel, M.; Engel, K.; Buchner, J. *The Journal of biological chemistry* **1993**, *268*, 1517-1520.

(6) Aquilina, J. A.; Shrestha, S.; Morris, A. M.; Ecroyd, H. *J Biol Chem* **2013**, *288*, 13602-13609.

(7) Ojha, J.; Masilamoni, G.; Dunlap, D.; Udoff, R. A.; Cashikar, A. G. *Mol Cell Biol* **2011**, *31*, 3146-3157.

(8) Cox, D.; Selig, E.; Griffin, M. D.; Carver, J. A.; Ecroyd, H. *The Journal of biological chemistry* **2016**.

(9) Cox, D.; Ecroyd, H. *Cell stress & chaperones* **2017**.

(10) Pivovarova, A. V.; Chebotareva, N. A.; Chernik, I. S.; Gusev, N. B.; Levitsky, D. I. *The FEBS journal* **2007**, *274*, 5937-5948.

(11) Pivovarova, A. V.; Mikhailova, V. V.; Chernik, I. S.; Chebotareva, N. A.; Levitsky, D. I.; Gusev, N. B. *Biochemical and biophysical research communications* **2005**, *331*, 1548-1553.

(12) Doshi, B. M.; Hightower, L. E.; Lee, J. *Ann N Y Acad Sci* **2010**, *1197*, 76-84.

(13) Garrido, C.; Bruey, J. M.; Fromentin, A.; Hammann, A.; Arrigo, A. P.; Solary, E. *FASEB journal : official publication of the Federation of American Societies for Experimental Biology* **1999**, *13*, 2061-2070.

(14) Houlden, H.; Laura, M.; Wavrant-De Vrieze, F.; Blake, J.; Wood, N.; Reilly, M. M. *Neurology* **2008**, *71*, 1660-1668.

(15) Evgrafov, O. V.; Mersiyanova, I.; Irobi, J.; Van Den Bosch, L.; Dierick, I.; Leung, C. L.; Schagina, O.; Verpoorten, N.; Van Impe, K.; Fedotov, V.; Dadali, E.; Auer-Grumbach, M.; Windpassinger, C.; Wagner, K.; Mitrovic, Z.; Hilton-Jones, D.; Talbot, K.; Martin, J. J.; Vasserman, N.; Tverskaya, S., et al. *Nature genetics* **2004**, *36*, 602-606.

(16) Muchowski, P. J.; Wacker, J. L. *Nature reviews. Neuroscience* **2005**, *6*, 11-22.

(17) Haslbeck, M.; Peschek, J.; Buchner, J.; Weinkauf, S. *Biochimica et biophysica acta* **2016**, *1860*, 149-166.

(18) McHaourab, H. S.; Godar, J. A.; Stewart, P. L. *Biochemistry* **2009**, *48*, 3828-3837.

(19) Hilton, G. R.; Lioe, H.; Stengel, F.; Baldwin, A. J.; Benesch, J. L. *Top Curr Chem* **2013**, *328*, 69-98.

(20) Basha, E.; O'Neill, H.; Vierling, E. *Trends Biochem Sci* **2012**, *37*, 106-117.

(21) Landry, J.; Lambert, H.; Zhou, M.; Lavoie, J. N.; Hickey, E.; Weber, L. A.; Anderson, C. W. *The Journal of biological chemistry* **1992**, *267*, 794-803.

(22) Arrigo, A. P. *Methods in molecular biology* **2011**, *787*, 105-119.

(23) Jovcevski, B.; Kelly, M. A.; Rote, A. P.; Berg, T.; Gastall, H. Y.; Benesch, J. L.; Aquilina, J. A.; Ecroyd, H. *Chem Biol* **2015**, *22*, 186-195.

(24) Theriault, J. R.; Lambert, H.; Chavez-Zobel, A. T.; Charest, G.; Lavigne, P.; Landry, J. *The Journal of biological chemistry* **2004**, *279*, 23463-23471.

(25) Heirbaut, M.; Lermyte, F.; Martin, E. M.; Beelen, S.; Verschueren, T.; Sobott, F.; Strelkov, S. V.; Weeks, S. D. *Arch Biochem Biophys* **2016**, *610*, 41-50.

(26) Hilton, G. R.; Hochberg, G. K.; Laganowsky, A.; McGinnigle, S. I.; Baldwin, A. J.; Benesch, J. L. *Philos Trans R Soc Lond B Biol Sci* **2013**, *368*, 20110405.

(27) Painter, A. J.; Jaya, N.; Basha, E.; Vierling, E.; Robinson, C. V.; Benesch, J. L. *Chem Biol* **2008**, *15*, 246-253.

(28) Benesch, J. L.; Aquilina, J. A.; Baldwin, A. J.; Rekas, A.; Stengel, F.; Lindner, R. A.; Basha, E.; Devlin, G. L.; Horwitz, J.; Vierling, E.; Carver, J. A.; Robinson, C. V. *Chem Biol* **2010**, *17*, 1008-1017.

(29) Horwitz, J.; Huang, Q. L.; Ding, L.; Bova, M. P. *Methods in enzymology* **1998**, *290*, 365-383.
(30) Bova, M. P.; Ding, L. L.; Horwitz, J.; Fung, B. K. *The Journal of biological chemistry* **1997**, *272*, 29511-29517.
(31) Kondrat, F. D.; Struwe, W. B.; Benesch, J. L. *Methods Mol Biol* **2015**, *1261*, 349-371.
(32) Ruotolo, B. T.; Benesch, J. L.; Sandercock, A. M.; Hyung, S. J.; Robinson, C. V. *Nat Protoc* **2008**, *3*, 1139-1152.
(33) Salbo, R.; Bush, M. F.; Naver, H.; Campuzano, I.; Robinson, C. V.; Pettersson, I.; Jorgensen, T. J.; Haselmann, K. F. *Rapid communications in mass spectrometry : RCM* **2012**, *26*, 1181-1193.
(34) Zhong, Y.; Han, L.; Ruotolo, B. T. *Angew Chem Int Ed Engl* **2014**, *53*, 9209-9212.
(35) Eschweiler, J. D.; Rabuck-Gibbons, J. N.; Tian, Y.; Ruotolo, B. T. *Anal Chem* **2015**, *87*, 11516-11522.
(36) Baldwin, A. J.; Lioe, H.; Robinson, C. V.; Kay, L. E.; Benesch, J. L. *J Mol Biol* **2011**, *413*, 297-309.
(37) Ecroyd, H.; Meehan, S.; Horwitz, J.; Aquilina, J. A.; Benesch, J. L.; Robinson, C. V.; MacPhee, C. E.; Carver, J. A. *Biochem J* **2007**, *401*, 129-141.
(38) Mymrikov, E. V.; Daake, M.; Richter, B.; Haslbeck, M.; Buchner, J. *J Biol Chem* **2017**, *292*, 672-684.
(39) Lanucara, F.; Holman, S. W.; Gray, C. J.; Eyers, C. E. *Nature chemistry* **2014**, *6*, 281-294.
(40) Benesch, J. L. *J Am Soc Mass Spectrom* **2009**, *20*, 341-348.
(41) Ghisaidoobe, A. B.; Chung, S. J. *Int J Mol Sci* **2014**, *15*, 22518-22538.
(42) Shashidharamurthy, R.; Koteiche, H. A.; Dong, J.; McHaourab, H. S. *The Journal of biological chemistry* **2005**, *280*, 5281-5289.
(43) Yin, S.; Xie, Y.; Loo, J. A. *J Am Soc Mass Spectrom* **2008**, *19*, 1199-1208.
(44) Daniel, J.; Friess, S.; Rajagopalan, S.; Wendt, S.; Zenobi, R. *Int J Mass Spectrom* **2002**, *216*, 1-27.
(45) Sluchanko, N. N.; Beelen, S.; Kulikova, A. A.; Weeks, S. D.; Antson, A. A.; Gusev, N. B.; Strelkov, S. V. *Structure* **2017**, *25*, 305-316.

Supporting Information for:

Evaluating the effect of phosphorylation on the structure and dynamics of Hsp27 dimers by means of ion mobility mass spectrometry

Blagojce Jovcevski[1], Megan A. Kelly[1], J. Andrew Aquilina[1], Justin L. P. Benesch[2] and Heath Ecroyd[1†]

[1]*Illawarra Health and Medical Research Institute and School of Biological Sciences, University of Wollongong, Wollongong, New South Wales 2522, Australia*

[2]*Department of Chemistry, Physical and Theoretical Chemistry Laboratory, South Parks Road, Oxford OX1 3QZ, United Kingdom*

[†]Correspondence to: heathe@uow.edu.au, +61-2-4221-3443

Supplemental Tables and Figures

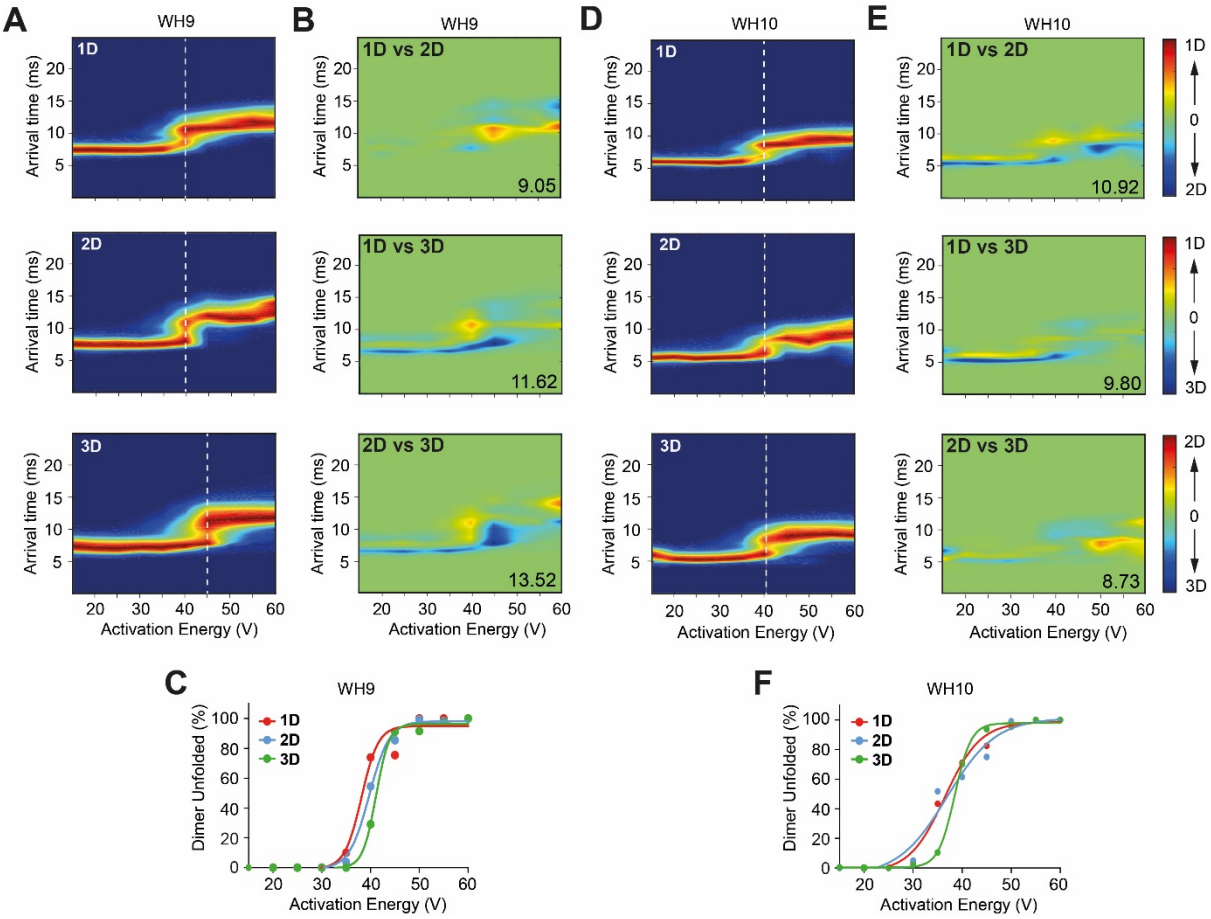

Figure S-1: Observing the differences in collision-induced unfolding dynamics of Hsp27$_M$ dimers by IM-MS at various wave heights. Related to Figure 4. ***A, D:*** The CIU of the Hsp27$_M$ dimer^{13+} (monitored via changes in the arrival time of species in the IM chamber) was examined with increasing activation energy (V). The heat maps indicate that no distinct intermediate species (i.e. no partially structured intermediate) between folded and unfolded states are present as the dimer unfolds in the gas-phase as a function of activation energy at various wave heights (WH: 9 V and 10 V). Across all wave heights, only a single unfolding transition is observed (*white dashed line*), indicating that both monomers (which are disulfide-linked via Cys137) unfold simultaneously in the gas-phase. ***B, E:*** Heat maps highlight the differences in the unfolding of the dimer^{13+} in the gas-phase between two isoforms at various wave heights (WH: 9 V and 10 V). RMSD values (%) (*bottom right corner*) indicate the difference in the unfolding of the dimer between each pair analysed (pairs analysed stated above in heat map scale where greatest difference attributed to one isoform indicated by either dark blue or red). The greatest difference in the unfolding dynamics was observed when Hsp27-1D and -2D were compared with Hsp27-3D. ***C, F:*** The

abundance of unfolded dimer (y-axis) was determined by tracking the loss of folded dimer with increased activation energy at various wave heights (WH: 9 V and 10 V). The Hsp27-3D dimer appears to be more stable (i.e. requires increased activation energy to reach 50% unfolded) compared to the –1D and -2D isoforms. CIU difference plots and RMSD values were calculated using CIUsuite with default settings [35].

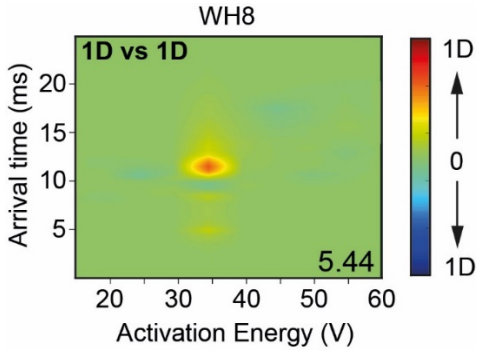

Figure S-2: Internal RMSD determination of the collision-induced unfolding dynamics of $Hsp27_M$ dimers by IM-MS. Related to Figure 4. CIU of $Hsp27_M$ dimers was monitored with increasing activation energy. Heat map highlights the differences in the unfolding of the $dimer^{13+}$ in the gas-phase between the same isoform (Hsp27-S15D; Hsp27-1D) calculated on two different occasions at the same WH (V). RMSD value (%) (*bottom right corner*) indicates the difference in the unfolding of the dimer between the pair analysed (pairs analysed where greatest difference attributed to one isoform indicated by either dark blue or red).

Table S-1: Arrival time analysis of Hsp27 dimers and 12mers by IM-MS. Related to Figure 3. Arrival time and peak width at half height of $Hsp27_M$ dimers and 12mers as determined by IM-MS. The increase in both arrival time and peak width at half height is indicative of an increase in the unstructured state of the species of $Hsp27_M$.

$Dimer^{13+}$	**Arrival time (ms)**			**Peak width at half height (ms)**		
	WH8	**WH9**	**WH10**	**WH8**	**WH9**	**WH10**
Hsp27-1D	9.87	7.31	5.9	1.68	1.42	0.92
Hsp27-2D	10.13	7.42	5.52	1.52	1.55	1.22
Hsp27-3D	10.39	7.38	5.9	1.8	2.18	1.76
$12mer^{31+}$	**Arrival time (ms)**			**Peak width at half height (ms)**		
	WH11.5		**WH13**	**WH11.5**		**WH13**
Hsp27-WT	13.07		9.23	2.1		1.17
Hsp27-1D	12.81		9.22	2.0		1.22
Hsp27-2D	12.81		9.22	2.0		1.29